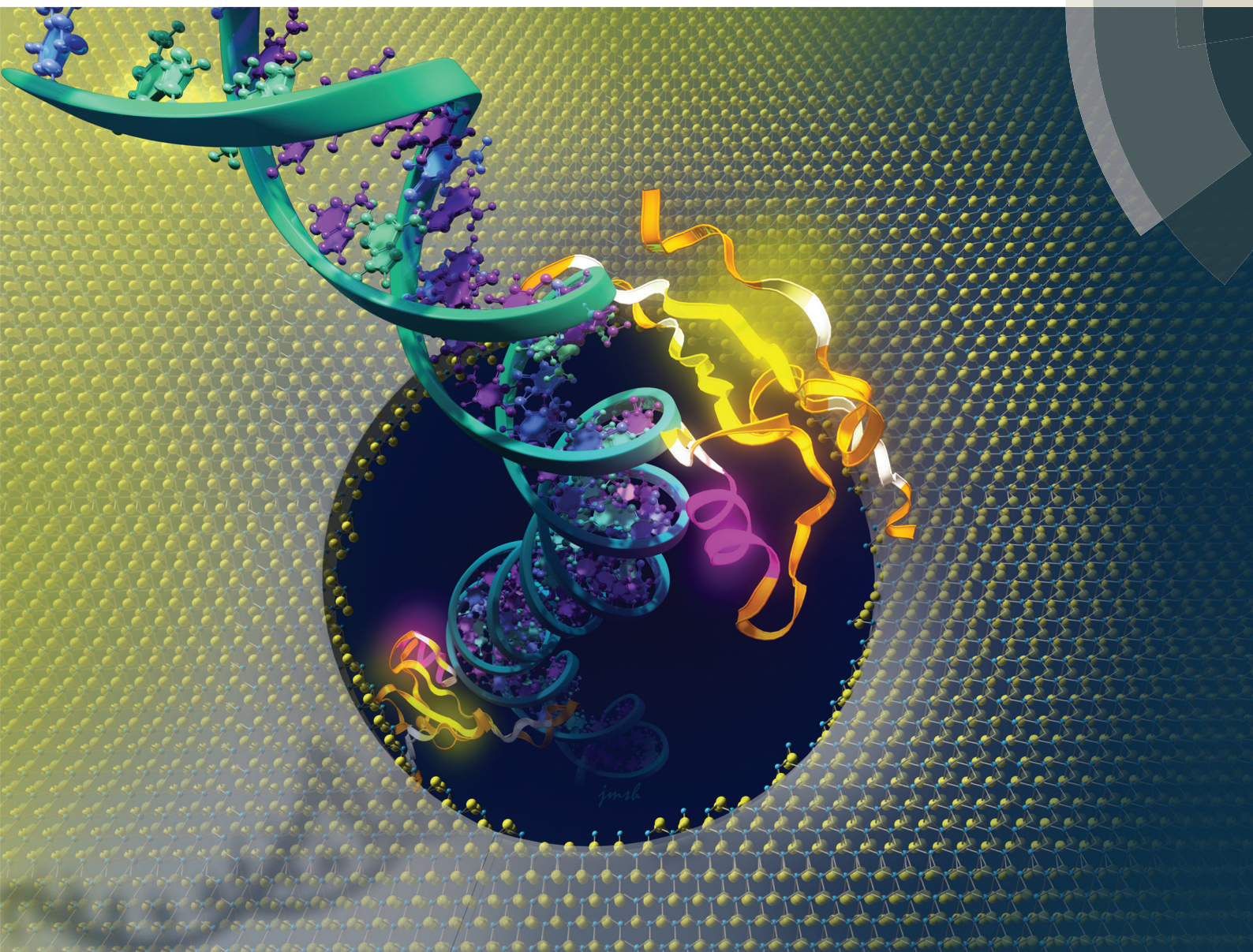


# Nanoscale

[rsc.li/nanoscale](http://rsc.li/nanoscale)



ISSN 2040-3372



PAPER  
Jiwook Shim, Rashid Bashir *et al.*  
Detection of methylation on dsDNA using nanopores in a MoS<sub>2</sub> membrane





Cite this: *Nanoscale*, 2017, **9**, 14836

## Detection of methylation on dsDNA using nanopores in a MoS<sub>2</sub> membrane†

Jiwook Shim,<sup>a</sup> Shouvik Banerjee,<sup>‡,b</sup> Hu Qiu,<sup>c</sup> Kirby K. H. Smithe,<sup>d</sup> David Estrada,<sup>e</sup> Julian Bello,<sup>a</sup> Eric Pop,<sup>d</sup> Klaus Schulten<sup>f</sup> and Rashid Bashir<sup>\*,g,h,i</sup>

Methylation at the 5-carbon position of the cytosine nucleotide base in DNA has been shown to be a reliable diagnostic biomarker for carcinogenesis. Early detection of methylation and intervention could drastically increase the effectiveness of therapy and reduce the cancer mortality rate. Current methods for detecting methylation involve bisulfite genomic sequencing, which are cumbersome and demand a large sample size of bodily fluids to yield accurate results. Hence, more efficient and cost effective methods are desired. Based on our previous work, we present a novel nanopore-based assay using a nanopore in a MoS<sub>2</sub> membrane, and the methyl-binding protein (MBP), MBD1x, to detect methylation on dsDNA. We show that the dsDNA translocation was effectively slowed down using an asymmetric concentration of buffer and explore the possibility of profiling the position of methylcytosines on the DNA strands as they translocate through the 2D membrane. Our findings advance us one step closer towards the possible use of nanopore sensing technology in medical applications such as cancer detection.

Received 1st May 2017,  
Accepted 20th July 2017

DOI: 10.1039/c7nr03092d

rscl.li/nanoscale

Cancer research is often centered around early detection and finding tumors before they metastasize. DNA methylation, defined as the addition or removal of a methyl group at the 5-position of the cytosine nucleotide, has been correlated to early carcinogenesis<sup>1–3</sup> with many promoter genes affected by aberrant methylation being linked to tumor formation.<sup>4–6</sup> In addition, high-throughput methylation analysis has unveiled that aberrant DNA methylation is correlated to both premalignant and malignant neoplasia.<sup>7–10</sup> Consequently, methylation pattern analysis in DNA can play a very critical role in the diag-

nosis of precancerous and early-stage cancer. However, current methods for analyzing genome-wide methylation rely heavily on bisulfite genomic sequencing.<sup>11</sup> This method requires a large sample volume due to DNA degradation during the bisulfite conversion and exhibits low PCR efficiency.<sup>5,12,13</sup> Previous studies have reported the feasibility of detecting cancer by methylation pattern analysis from genomic extracts of human bodily fluids such as plasma, serum, urine, and stool.<sup>5,14,15</sup> However, only a minuscule amount of methylated DNA can be obtained from body fluids.<sup>13</sup> As a result, most conventional methylation assays are not suitable for detecting the extremely low level of methylated DNA in bodily fluids. This presents a need for a less labor intensive and direct method to characterize methylation. Our previous work has successfully investigated the possibility of nanopore-based devices for detection of hypermethylation, coarse quantification of methylation sites, and coarse profiling of single dyad methylation patterns. Thus, we believe that the nanopore technology holds significant promise for the detection of methylation for precancerous and early-stage cancer.<sup>16,17</sup>

Nanopore technology is a cost-effective, high-throughput platform that could assist in various medical applications such as immunoisolation, biocapsules, drug delivery devices, and targeted biorecognition platforms.<sup>18</sup> Solid-state nanopores are favorable because they can operate in various liquid media and pH conditions as well as their production being scalable and compatible with other detection techniques<sup>19–21</sup> and other nanofabrication techniques.<sup>22,23</sup> However, certain obstacles, such as controlling translocation time and discriminating

<sup>a</sup>Department of Biomedical Engineering, Rowan University, Glassboro, NJ 08028, USA. E-mail: shimj@rowan.edu; Tel: +1 856-256-5393

<sup>b</sup>Department of Material Science and Engineering, University of Illinois at Urbana – Champaign, Urbana, IL 61801, USA

<sup>c</sup>State Key Laboratory of Mechanics and Control of Mechanical Structures, Nanjing University of Aeronautics and Astronautics, Nanjing, 210016, China

<sup>d</sup>Department of Electrical Engineering, Stanford University, Stanford, CA 94305, USA

<sup>e</sup>Department of Material Science and Engineering, Boise State University, Boise, ID 83725, USA

<sup>f</sup>Department of Physics and Beckman Institute, University of Illinois at Urbana – Champaign, Urbana, IL 61801, USA

<sup>g</sup>Department of Bioengineering, University of Illinois at Urbana – Champaign, Urbana, IL 61801, USA. E-mail: rbashir@illinois.edu; Tel: +1 217-333-1867

<sup>h</sup>Micro and Nanotechnology Laboratory, University of Illinois at Urbana – Champaign, Urbana, IL 61801, USA

<sup>i</sup>Carle Illinois College of Medicine, University of Illinois at Urbana – Champaign, Urbana, IL 61801, USA

†Electronic supplementary information (ESI) available. See DOI: 10.1039/c7nr03092d

\*These authors contributed equally to this work.



between bases and proteins, introduce complications that limit the commercial use of solid-state nanopores. In particular, they tend to exhibit relatively lower single molecule detection sensitivity due to the thickness of conventional membranes and inconsistent surface charge distribution.<sup>22,24,25</sup> Although solid state nanopores yield low ionic current signal-to-noise ratios, graphene nanopores, in theory, can exhibit favorable detection sensitivity when compared to other solid-state nanopores such as  $\text{SiN}_x$ .<sup>26</sup> Also, it has been predicted computationally that nanopores on 2D materials such as graphene and  $\text{MoS}_2$  are capable of detecting and mapping DNA methylation with high resolution and accuracy.<sup>59</sup> In this paper, we explore the translocation of naked double-stranded DNA (dsDNA) and a methylated dsDNA-MBP complex through nanopores drilled in a two-dimensional molybdenum disulfide ( $\text{MoS}_2$ ) membrane. In addition, to attest to its viability as an alternative to graphene nanopores, we also present experiments with a buffer of asymmetric molarity to slow down the translocation of biomolecules through the pore.

## Results and discussion

### Fabrication and current-voltage signature of the nanopores in $\text{MoS}_2$

Solid-state nanopores can be used as inexpensive and high-performance biosensors that are capable of the single molecule detection of a wide variety of analytes of medical interest, ranging from small molecules to post-translationally modified proteins.<sup>27</sup> Specifically, the nanopore biosensing platform has become especially attractive in the realm of DNA sequencing.<sup>22,28</sup> Nanopores use the principle of ionic current spectroscopy to electrically distinguish the unique current blockage signatures of each nucleotide base.<sup>16,29</sup> Theoretically, the graphene nanopore of 1.6 nm would read the transverse conductance of the translocating DNA and could lead to an error-free read-out.<sup>30</sup> Atomically small graphene nanopores, closely resembling the diameter of dsDNA, have a high sensitivity to infinitesimal changes in the outer diameter of the translocating DNA.<sup>31</sup> These nanopores can resolve nanoscale-spaced molecular structures with a resolution of less than 0.6 nm along the length of the molecule. However, the unique density of the states of graphene and the absorption of water molecules are factors that could introduce error into graphene nanopore readings.<sup>30</sup> More importantly, graphene nanopores have a strong hydrophobic interaction with ssDNA, which causes the DNA to attach to the graphene membrane and impedes translocation.<sup>32</sup> To overcome this, the surface of the graphene membrane often must be treated with agents such as 16-mercaptohexadecanoic acid in 8:2 toluene/ethanol to demote DNA adhesion and promote translocation.<sup>24,33,34</sup>

Alternative materials have been explored to eliminate the need for additional surface treatment protocols.<sup>22</sup> Molybdenum disulfide is a novel atomically thin material that has been recognized as a possible alternative to graphene. As shown by Gaur *et al.*,  $\text{MoS}_2$  membranes grown below 900 °C

exhibit high surface energy and a semi-crystalline structure that is associated with a decreased hydrophobicity and increased wetting.<sup>35</sup> The less hydrophobic surface nature of the  $\text{MoS}_2$  grown under optimal conditions allows for successful threading of dsDNA of different lengths and conformations, displaying superior yields.<sup>24</sup>  $\text{MoS}_2$  nanopores also exhibit a lower failure rate in high ionic strength solutions,<sup>24</sup> and show four distinct ionic current signals for four homonucleobases.<sup>22</sup> Unlike graphene, the semiconducting bandgap of  $\text{MoS}_2$  is independent of the width of the nano-ribbon and can allow for detection of changes in the potential induced in the liquid environment due to the translocation of the DNA.

Fig. 1a illustrates the layout of the  $\text{MoS}_2$  nanopore structure that we have fabricated. The free standing  $\text{MoS}_2$  monolayer was situated on a 12 mm × 12 mm substrate structure consist-

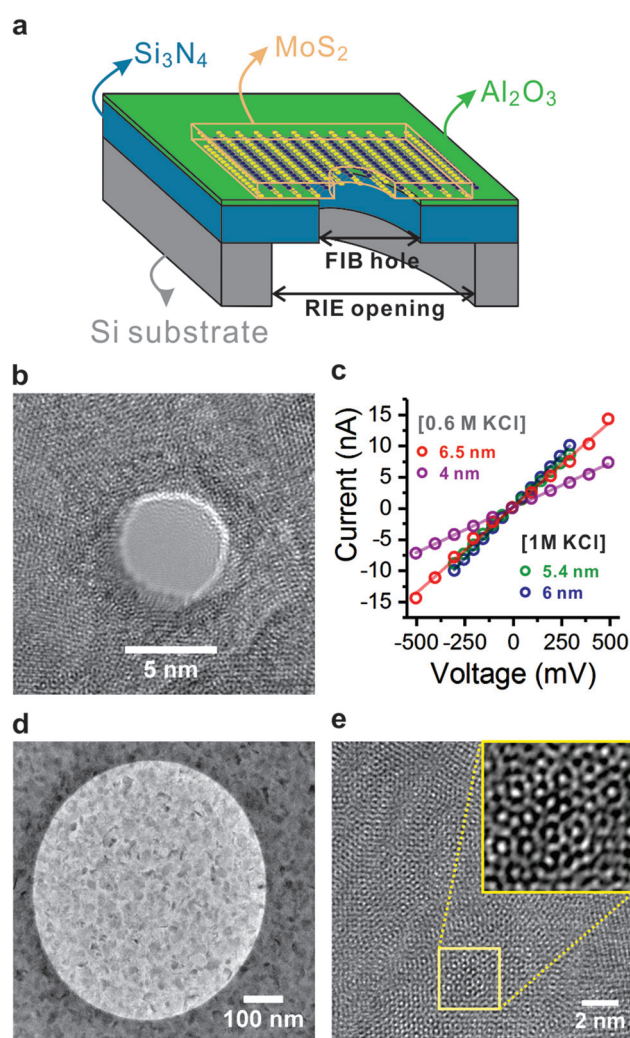


**Fig. 1** (a) Schematic illustrates the  $\text{MoS}_2$  nanopore structure. (b) TEM image of a typical 6 nm  $\text{MoS}_2$  nanopore. (c)  $I$ - $V$  characteristic of  $\text{MoS}_2$  nanopores in KCl solution at pH 7.2 containing 10 mM Tris and 1 mM EDTA. (d) TEM image shows that the  $\text{MoS}_2$  layer covers the entire FIB pore of 600 nm diameter. (e) HRTEM shows a honeycomb-like  $\text{MoS}_2$  membrane structure (inset shows a zoomed-in image of the yellow square).

ing of 300 nm thick  $\text{SiN}_x$  and 20 nm thick  $\text{Al}_2\text{O}_3$  that were deposited using PECVD (plasma enhanced chemical vapor deposition) and ALD (atomic layer deposition). An 80-micron hole was opened on the backside of the silicon substrate using DRIE (deep reactive ion etching), and a concentric  $\sim 500$  nm hole was subsequently opened through the  $\text{Al}_2\text{O}_3$  using a FIB (focused ion beam) (see the ESI† for the detailed process). The  $\text{MoS}_2$  membrane was grown using CVD (chemical vapor deposition) and transferred to the device, as described in the ESI,† and the  $\text{MoS}_2$  nanopore was subsequently drilled using TEM (transmission electron microscopy) as described in the Materials and methods section. Fig. 1b shows the TEM image of a typical  $\sim 6$  nm  $\text{MoS}_2$  nanopore. Nanopores for this experiment were created between 4 nm and 6.5 nm in diameter, and the current–voltage characteristics of the  $\text{MoS}_2$  nanopores were determined in both 1 M KCl and 0.6 M KCl as shown in Fig. 1c. Fig. 1d shows a TEM image of a free standing  $\text{MoS}_2$  membrane over the FIB hole that confirms no defects were present on the membrane before drilling of the nanopore on the  $\text{MoS}_2$  membrane. Also, high-resolution transmission electron microscopy (HRTEM) showed a honeycomb-like image that is unique to  $\text{MoS}_2$ , thus confirming that the  $\text{MoS}_2$  membrane was properly grown by the CVD method, as shown in Fig. 1e. Additional characterization was performed to analyze the quality of the  $\text{MoS}_2$  membrane using Raman Spectroscopy, as described in the ESI.† The thickness of the  $\text{MoS}_2$  membrane was examined by atomic force microscopy (AFM) as shown in the ESI.† The height profile indicates that the thickness of the CVD grown  $\text{MoS}_2$  membrane corresponds to the thickness of a single  $\text{MoS}_2$  layer.

### Detection of 10 kb double-stranded DNA

To examine the feasibility of translocating dsDNA through a  $\text{MoS}_2$  nanopore, random sequences of 10 kb dsDNA were introduced into a 6.5 nm  $\text{MoS}_2$  nanopore. The dsDNA sequences were transported through the  $\text{MoS}_2$  nanopore at various voltages in the buffer solution of 0.6 M KCl at pH of 7.2 containing 10 mM Tris and 1 mM EDTA. Representative data traces of 10 kb dsDNA transports at 500 mV, 700 mV, and 1000 mV are shown in Fig. 2a–c. Distinct downward current blockages were observed in each of the data traces, undeniably confirming that the dsDNA transported through the  $\text{MoS}_2$  nanopore. Fig. 2d shows a scatter plot of all 10 kb transport events at the displayed voltages. The data trace of 700 mV displayed higher dsDNA transport occurrence than that of the data trace of 500 mV, and the 1000 mV data trace showed more than that of the 700 mV data trace as expected. The higher occurrence of the dsDNA transport with increasing voltage is in agreement with the previous observations of dsDNA transports in  $\text{SiN}_x$ .<sup>16</sup> To further investigate the dsDNA transport through the  $\text{MoS}_2$  nanopore, the current blockages and the translocation duration were analyzed. To obtain the current blockage values of dsDNA transports, a histogram built with blocked current data produced by dsDNA transports was fitted with a Gaussian function as shown in Fig. 2e. The current blockages of 10 kb dsDNA through a 6.5 nm  $\text{MoS}_2$  nanopore were  $1.27 \pm 0.24$  nA at 500 mV,  $1.7 \pm 0.41$  nA at 700 mV, and  $2.35 \pm 0.43$  nA at

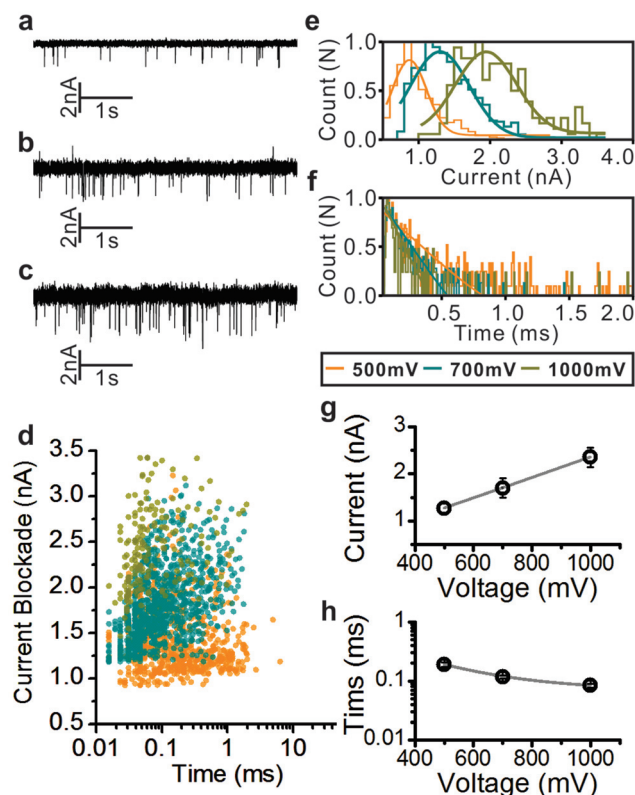


**Fig. 2** (a) Data trace of the 10 kb dsDNA transport at 500 mV. (b) Data trace of the 10 kb dsDNA transport at 700 mV. (c) Data trace of the 10 kb dsDNA transport at 1000 mV. (d) Scatter plot of the 10 kb dsDNA transport in the 6.5 nm  $\text{MoS}_2$  nanopore at 600 mM KCl solution (pH 7.2) containing 10 mM Tris and 1 mM EDTA. (e) Current blockage histogram fitted with the Gaussian function. (f) Transport duration histogram fitted with the exponential decay function. (g) Current blockages of DNA transports fitted with the linear function. The current blockage at 500 mV was  $1.27 \pm 0.24$  nA, 700 mV was  $1.7 \pm 0.41$  nA, and 1000 mV was  $2.35 \pm 0.43$  nA. (h) Transport durations of DNA transports fitted with the exponential decay function. The transport duration at 500 mV was  $188 \pm 17$   $\mu\text{s}$ , 700 mV was  $118 \pm 8$   $\mu\text{s}$ , and 1000 mV was  $83 \pm 6$   $\mu\text{s}$ .

1000 mV. The amplitudes of the current blockages were increased at higher biased voltages as shown in Fig. 2g, in agreement with the trends of dsDNA transport observed in other nanopores.<sup>36,37</sup> Fig. 2f shows the transport duration values of the dsDNA which were obtained by fitting an exponential decay function to the dsDNA transport dwell time histograms. As expected, an accelerated transport velocity was observed at higher biased voltages. The transport durations were  $188 \pm 17$   $\mu\text{s}$  at 500 mV,  $118 \pm 8$   $\mu\text{s}$  at 700 mV, and  $83 \pm 6$   $\mu\text{s}$  at 1000 mV as shown in Fig. 2h. As observed in the dsDNA transport in other material nanopores,<sup>16,36,37</sup> a higher voltage generally yielded a stronger blockage current, but shorter transport duration times. Findings with 10 kb dsDNA transports through the 6.5 nm  $\text{MoS}_2$  nanopore were in concordance with the observations in previous studies. Molecular dynamics (MD) simulations also demonstrated larger current blockages and reduced transport duration by transporting dsDNA through a  $\text{MoS}_2$  nanopore at higher voltages as shown in the ESI,† thus validating our experimental findings. Previous

studies have indicated the challenges of dsDNA transport through graphene nanopores due to the affinity of the graphene surface to the DNA causing the DNA strand to adhere to the surface of the nanopore membrane.<sup>36</sup> Such a difficulty was not observed on dsDNA transports through the MoS<sub>2</sub> nanopore in our studies as it was much less difficult to wet the nanopore membrane. However, a higher biased voltage, greater than 800 mV, can enlarge the open pore in the MoS<sub>2</sub> nanopore<sup>38</sup> as was evident in a previous study after recording DNA transports at 1000 mV. Also, the enlarging of the MoS<sub>2</sub> nanopore can be seen in Fig. 2b and c, where occasional upward spikes and increased noise levels at 700 mV and 1000 mV are demonstrated. We have tested the current–voltage characteristic before and after applying 1000 mV, and the result indicates that the MoS<sub>2</sub> nanopore can be enlarged through an electrochemical reaction (ESI†).

### Detection of naked and methylated dsDNA fragments

DNA methylation patterns are often correlated to tumor formation and cancer progression. In particular, previous studies reported that hypermethylation is associated with many types of cancer and potentially correlated with metastasis in many other tumor types.<sup>5,6,39–41</sup> Previous studies have also demonstrated that nanopore sensors cannot discriminate between methylated DNA and unmethylated DNA without labeling of some sorts.<sup>16</sup> One method to utilize nanopore technology to detect methylation is to attach methyl binding proteins (MBPs) to methylated DNA. MBPs selectively bind to methylcytosine bases on methylated DNA, thereby confirming its presence in the sequence.<sup>16,17</sup> Our previous studies have presented the selective labeling of methylated sites on dsDNA using MBPs. Herein, we used the same strategy and DNA with the same methylated pattern to show the ability of the MoS<sub>2</sub> nanopore to discriminate naked DNA from hypermethylated DNA (hyMethDNA). Target DNAs were 90 bp sequences with 30 CpG sites. No methylation was added to the naked DNA and 10 methylcytosine domains were added on hypermethylated DNA to have uniformly distributed methylation sites. For our experiment, a nanopore with a diameter of 7.2 nm was used for the detection of the 90 bp dsDNA fragments in our nanopore experimental setup of 1 M KCl at pH 7.2 containing 10 mM Tris and 1 mM EDTA. We first examined the detection of 90 bp naked dsDNA through a MoS<sub>2</sub> nanopore at 200 mV to prevent the MoS<sub>2</sub> nanopore from damage resulting from the enlargement of the nanopore at a high biased voltage. However, translocation events under these conditions were unnoticeable. Interestingly, upon lowering the applied voltage to 100 mV, transport events for the 90 bp dsDNA were observed. It was surprising to see the transport of dsDNA through MoS<sub>2</sub> at these low biased voltages as other membranes typically require higher voltages to reveal translocation events. Representative transport sample events of the 90 bp dsDNA fragments through a MoS<sub>2</sub> nanopore are displayed in Fig. 3a, b, and c for applied voltages of 50 mV, 80 mV, and 100 mV, respectively. To date, SiN<sub>x</sub> and graphene nanopore experiments have not reported dsDNA transport below 200 mV.

The possible explanations for the lack of transportation data with these commonly used membranes could be the negative surface charge of the SiN<sub>x</sub> membrane and the hydrophobic surface affinity to graphene causing DNA to adhere. This is especially relevant for the nanopores in SiN<sub>x</sub> membranes ranging from 10–30 nm in thickness, where a smaller pore diameter than the membrane thickness results in a pore that behaves like a nanochannel, increasing the entropic barrier that the DNA molecule needs to overcome to result in translocation. Since the isoelectric point of SiN<sub>x</sub> is ~4 and negatively charged in experimental solution at pH 7.2,<sup>42</sup> the dsDNA would possibly be repelled at bias voltages under 200 mV. In comparison, a pore in a thin MoS<sub>2</sub> 2D membrane does not repel dsDNA. The values of the transport current blockage and transport duration were obtained by fitting a Gaussian function, and an exponential decay function to the blocked current histogram and transport dwell time histogram, respectively, as demonstrated in Fig. 3d and e. Short DNA fragments, such as the 90 bp, have very fast translocations at high voltages, thus rendering them undetectable. Hence, low biased voltage levels were used to detect these fragments. The longer DNA fragments, such as the 10 kb, were still detectable at higher applied voltages. Generally, increasing applied biased voltage increases translocation speed and makes it difficult to detect short DNA sequences. Adjusting the applied voltage to the specific length of the molecule in question can help assure a more accurate reading.

The MoS<sub>2</sub> nanopore of 7.2 nm in diameter could detect 90 bp dsDNA, with blocked currents of  $282 \pm 22$  pA at 50 mV,  $312 \pm 13$  pA at 80 mV, and  $376 \pm 16$  pA at 100 mV as shown in Fig. 3f and times of  $53 \pm 3$   $\mu$ s at 50 mV,  $36 \pm 4$   $\mu$ s at 80 mV, and  $32 \pm 2$   $\mu$ s at 100 mV as shown in Fig. 3g. The increase in the bias voltage to the original 200 mV did not result in noticeable transport events as demonstrated in Fig. 3h. However, the addition of hyMethDNA bound to MBD1x produced detectable events as shown in Fig. 3i. Representative sample events of the hyMethDNA/MBD1x complex through the MoS<sub>2</sub> nanopore are presented in Fig. 3j. To form the complex of hyMethDNA and MBD1x, the two molecules were mixed and incubated at room temperature for 15 minutes before experiments. While recording when naked DNA was in the solution and no translocations were observed, hyMethDNA fully bound to MBD1x were introduced into the chamber. Surprisingly, the hyMethDNA with MBPs displayed a signature current blockage as shown in Fig. 3j and were selectively detected at 200 mV. It can be inferred that the complex translocated through the pore slower than naked DNA due to the altered larger physical dimension brought about by annexing 10 MBD1x on the dsDNA fragment, in addition to the positive net charge of the MBD1x on the DNA reducing the overall charge on the complex. The isoelectric point of MBD1x is known to be 8.85,<sup>43</sup> thus it would be positively charged in the solution with pH 7.2. Not only does this serve as a confirmation of the presence of a methylcytosine base on the DNA sequence and the affinity of the MBP to the methyl group, but it also alludes to the ability of MoS<sub>2</sub> nanopores in detecting methylated DNA. The structure



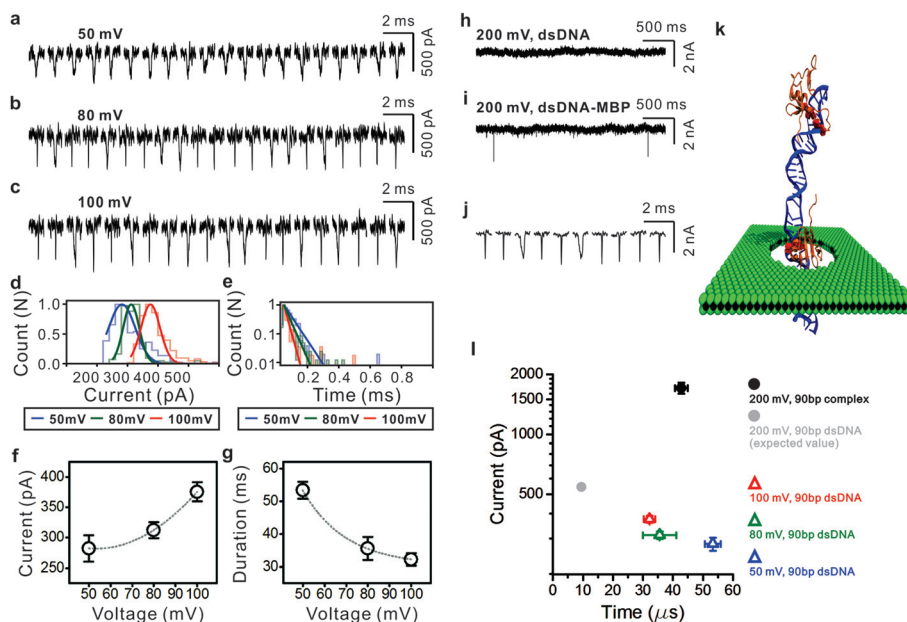


**Fig. 3** (a) Sample events of 90 bp dsDNA transports at 50 mV biased voltage in the 7.2 nm MoS<sub>2</sub> nanopore. (b) Sample events of 90 bp dsDNA transports at 80 mV biased voltage in the 7.2 nm MoS<sub>2</sub> nanopore. (c) Sample events of 90 bp dsDNA transports at 100 mV biased voltage in the 7.2 nm MoS<sub>2</sub> nanopore. (d) Current blockage histogram in the function of biased voltages. (e) Blocked current duration histogram in the function of biased voltages. (f) Current blockage of transports. The values are obtained by fitting the Gaussian function to the current blockage histogram. The current blockage at 50 mV was  $282 \pm 22$  pA, 80 mV was  $312 \pm 13$  pA, and 100 mV was  $376 \pm 16$  pA. (g) Blocked current duration of transports. The values are obtained by fitting the exponential decay function to the blocked current duration histogram. The transport duration at 50 mV was  $53 \pm 3$   $\mu$ s, 80 mV was  $36 \pm 4$   $\mu$ s, and 100 mV was  $32 \pm 2$   $\mu$ s. (h) Current trace of the 90 bp dsDNA transport at 200 mV biased voltage in the 7.2 nm MoS<sub>2</sub> nanopore. Momentary transport duration of short DNA is beyond the detection limit of the measurement device, consequently transports of 90 bp dsDNA were undetectable. (i) Current trace of 90 bp methylated dsDNA-MBP transports at 200 mV biased voltage in the 7.2 nm MoS<sub>2</sub> nanopore. (j) Sample events of 90 bp methylated dsDNA-MBP transports at 200 mV in the 7.2 nm MoS<sub>2</sub> nanopore. (k) Still image of molecular dynamics simulation showing the methylated dsDNA-MBP complex transport through the MoS<sub>2</sub> nanopore. (l) Transport data comparison between dsDNA and methylated DNA-MBP.

of the complex is presented in Fig. 3k to illustrate methylation and the presence of MBD1x in the DNA. The unmeasurable naked dsDNA transport events at 200 mV (Fig. 3i) can be explained by translocation that was too rapid. The DNA translocation duration time was demonstrated to decrease at higher voltages in a voltage-dependent manner. Fitting with an exponential decay function (ESI<sup>†</sup>) shows the expected value of the translocation of the 90 bp dsDNA transport at 200 mV to be  $\sim 10$   $\mu$ s, which is close to the data acquisition time interval of 10  $\mu$ s of the experimental setup (see the Materials and methods section), and hence was likely out of the measurement range. Fig. 3l shows the obtained current blockage and transport durations of the naked DNA and hyMethDNA/MBD1x complex along with the expected current blockage and duration of the 90 bp dsDNA fragment transport at 200 mV, which is unnoticeable under our experimental recording conditions.

#### Slowing down the dsDNA transport and detection of a single CpG site in a dsDNA fragment

Hypomethylation, the loss of methylation in DNA when compared to normal levels, is another major epigenetic modification in cancer cells. The pattern of DNA epigenetic alterations in cancer varies from the individual CpG dyad at the

local level, to methylation in 1 million base pairs, to DNA demethylation during carcinogenesis. This results in a loss of methylation on both strands *via* the possible intermediates of hemimethylated dyads.<sup>44</sup>

However, conventional methylation assays such as methylation-specific PCR is technically limited and challenging for the diagnosis of DNA hypomethylation.<sup>45</sup> Although our previous study demonstrated discrimination between hypomethylated DNA and individual CpG dyads at the center of the sequences by labeling with MBP, detection of the methylation pattern using a thick SiN<sub>x</sub> membrane was not possible.<sup>17</sup> In that study, the single MBP was in the middle of the molecule and the electrical peak indicating the methylation location was broad. Herein, we report the methylation detection of dsDNA through a MoS<sub>2</sub> nanopore with a slow translocation velocity due to an asymmetric salt gradient.<sup>46</sup> Longer translocations can allow for high-resolution measurements to distinguish individual nucleotide bases.<sup>47</sup> Various strategies, from applying gel media on the *cis* or *trans* side of the membrane, to varying voltages or buffer solution concentration gradients, have been implemented to slow the translocation and suspend DNA strands in the pore.<sup>47,48</sup> For our experiment, we used an asymmetric buffer solution of 0.6 M KCl on the *cis* side of the membrane and 3 M KCl on the *trans* side. Our MoS<sub>2</sub> nano-

pore-based methylation assay demonstrates the detection of a single methylation CpG dyad site at the end of 90 bp dsDNA. We utilized the MBD1x and chose a single methylation CpG dyad to check the viability of the MoS<sub>2</sub> nanopore for the detection of hypomethylated DNA. The target DNA fragments were designed to have a single CpG dyad methylated site near the end of the strand, 84<sup>th</sup> to 87<sup>th</sup> bases in 90 bp dsDNA (endMethDNA). Both naked DNA and the endMethDNA bound to a single MBD1x were used for translocation experiments in a 9 nm MoS<sub>2</sub> nanopore and both displayed measurable current blockade signatures as shown in Fig. 4a. Samples of 90 bp naked DNA (Fig. 4a top) and MBD1x bound endMethDNA (Fig. 4a bottom) are shown in Fig. 4a and the corresponding scatter plot is shown in Fig. 4b. The transport current blockage values of both naked DNA,  $-277 \pm 20$  pA, and the complex,  $-600 \pm 66$  pA, were obtained using a Gaussian function as shown in Fig. 4c. The translocation times of the naked DNA and endMethDNA/MBD1x were also obtained by fitting a Gaussian function to the transport dwell time histogram as shown in Fig. 4d. In comparison with the dsDNA transport in symmetric 1 M KCl shown in Fig. 3, using an asymmetric salt gradient significantly slowed down the transport duration of 90 bp naked DNA. Although direct comparison is not appropriate due to the large diameter of the nanopore used for this experiment, naked DNA was successfully detected with a duration time of  $1.23 \pm 0.21$  ms at 200 mV. The Gaussian function used to fit this data differs from the one used under symmetric salt conditions as asymmetric salt gradients have been shown to fit to different functions.<sup>49</sup> In comparison with the expected transport shown in Fig. 3l, the transport was slowed down  $\sim 100$ -fold. The endMethDNA bound to a single MBD1x translocated through the MoS<sub>2</sub> nanopore at  $1.39 \pm 0.23$  ms, which was a  $\sim 160$   $\mu$ s slower translocation than the naked DNA. While we had previously found a  $\sim 20$ -fold difference between naked DNA and locally methylated DNA through SiN<sub>x</sub> nanopores, a similar range of translocation duration between naked DNA and endMethDNA was unexpected. However, a similar range of transport duration between naked DNA and endMethDNA/MBD1x can be explained. The negatively charged inner wall of a 10 nm thick SiN<sub>x</sub> nanopore is likely to interact with the positively charged methyl-binding protein during transportation, whereas a 2-D material MoS<sub>2</sub> nanopore is unlikely to interact during transportation. In addition, compared to hyMethDNA fully bound to MBD1x, endMethDNA possesses only one MBD1x. Thus the overall charge on the molecule is not perturbed. Consequently, the 90 bp naked DNA and endMethDNA would not be significantly different in the transport duration in the 2D MoS<sub>2</sub> membranes. The main factor impeding the complex transport through a MoS<sub>2</sub> nanopore is a biased positive voltage. A demonstration of atomic-scale translocation dynamics of the complex through a MoS<sub>2</sub> nanopore is shown in the ESI.† To further analyze the whole data set for the current blockade and transport duration, a box-and-whisker plot was adopted. Fig. 4e shows that most current blockages of naked DNA fall in  $-276 \pm 20$  pA, and endMethDNA/MBD1x showed two distinct current blockage levels; shallow at  $-251 \pm$

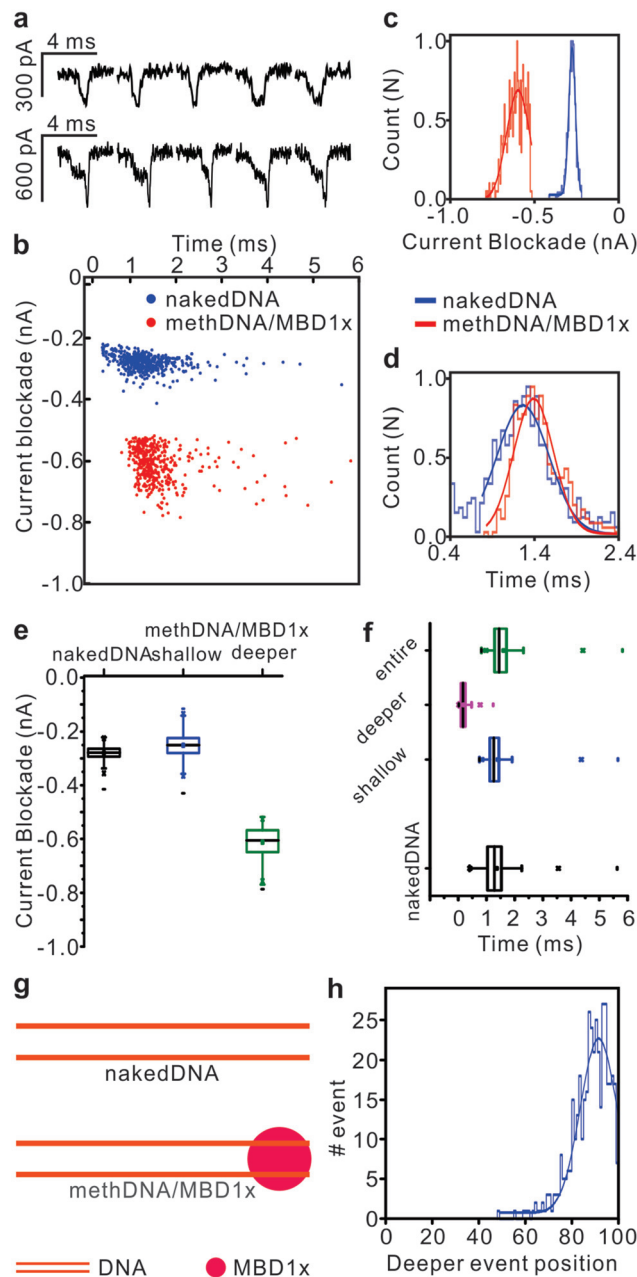


**Fig. 4** (a) Sample transport events of naked DNA (top) and terminal-methDNA/MBD1x (bottom) in asymmetric solution. (b) Scatter plot of transport events. Blue dots represent the naked DNA transport and red dots represent the complex. (c) Current blockade histogram of naked DNA (blue) and complex (red) transports. (d) Transport duration histogram of naked DNA (blue) and complex (red) events. (e) Box chart of current blockades. The current blockade of naked DNA is shown in black,  $276 \pm 20$  nA, the DNA region of the complex (shallow) is in blue,  $251 \pm 39$  nA, and the DNA/protein region (deeper) in green,  $600 \pm 66$  nA. (f) Box chart of transport durations. The transport duration of naked DNA is shown in black,  $1.23 \pm 0.21$  ms, the DNA region of the complex (shallow) in blue,  $1.25 \pm 0.17$  ms, the DNA/protein region (deeper) in red,  $0.138 \pm 0.11$  ms, and the entire complex in green,  $1.39 \pm 0.23$  ms. (g) Schematic shows scaled dsDNA and the methDNA/MBD1x complex. (h) Methylation site detection shows that most complex transports end with terminal-protein. It is hypothesized that negatively charged DNA enters the nanopore by an applied positive voltage and the transport ends with protein.

39 pA and deeper at  $-600 \pm 66$  pA. The shallow current blockage is at similar levels of transport current blockages to that of naked DNA, thus corresponding to the transport of the DNA region on the complex. The deeper current blockages are associated with the transport of MBD1x on the DNA through the nanopore. The  $\sim 3$ -fold increased current blockage by the MBP region is on the same order of magnitude as the current blockage found in previous studies as well.<sup>16</sup> The transport duration of naked DNA and endMethDNA bound to MBD1x is shown in Fig. 4f. The transport of the MBP region on the DNA took  $0.138 \pm 0.11$  ms. This translates to 10% of the entire complex translocation over a 1.39 ms period. Comprehensively, the MoS<sub>2</sub> nanopore can detect the methylation site more precisely than the SiN<sub>x</sub> membrane. The schematic in Fig. 4g illustrates dsDNA and endMethDNA bound to MBD1x. Slowed translocation times were observed by varying the buffer concentration.

Methylation site detection shown in Fig. 4h revealed that translocation events with the methylated DNA/MBD1x complex ended with the terminal protein instead of leading with it. It can be inferred from this finding that the positively charged MBD1x near the nanopore is always repelled by the positively applied bias voltage and will spin to the origin while the DNA region of the complex is being pulled into the nanopore. Consequently, all of the endMethDNA/MBD1x transport into the pore occurred in a fixed orientation, which included the DNA entering first and the protein complex lagging behind. From this, it can be assumed that the negatively charged DNA that was used for the study was attracted by the applied positive charge and pushed towards the nanopore ahead of the region where MBD1x was attached. This was confirmed through the detection of methylation locations using the MoS<sub>2</sub> nanopore, but also applies to other nanopores such as SiN<sub>x</sub>. The occurrence of a deeper current blockage was mainly observed at the end of the whole complex transport, as shown in Fig. 4h. The abscissa represents the length of the entire complex translocation, normalized and recalculated as 100%. The peak occurrence of the deeper current blockage was obtained by fitting a Gaussian function to the occurrence histogram. The fitting value was  $90.5 \pm 3\%$ , which indicates the deeper current blockages mainly occurring at the end of the entire complex translocation. This result suggests that the position of methylation on dsDNA can be more precisely detected using nanopores in thin membranes.

## Conclusions

We investigated the use of the MoS<sub>2</sub> nanopore for dsDNA translocation and methylation detection experiments. Detection of methylcytosine bases has been reported previously with SiN<sub>x</sub> and graphene nanopore sensors, but MoS<sub>2</sub> presents several favorable and specific characteristics that could make it a more viable and robust option than the more commonly used membranes. These characteristics include the ability to produce a small nanopore on a thin membrane while retaining good

signal-to-noise ratios and no need for surface treatment to reduce hydrophobic surface interactions as is necessary for graphene membranes. After determining that dsDNA translocation was possible through MoS<sub>2</sub>, we also showed that dsDNA translocation could be slowed by using an asymmetric concentration of buffer solutions to provide higher spatial resolution. We demonstrated the detection of single MBD1x proteins in a site-specific manner which could be used to distinguish the location of the methyl cytosine nucleotide base on the DNA sequence. We also hypothesized that the charge of the DNA strand coupled with the applied voltage allows one to control the orientation of the translocating DNA strand.

Being able to detect aberrant methylation in a routine lab screening could help identify cancer signatures at various stages or progression. This could prove crucial regarding early intervention and therapy and ultimately lead to an increase in the rate of survival. Work remains to be accomplished in the control of translocation speeds, resolution of signature current blockades, and in profiling the location of attached MBPs. We hope that this work serves as a springboard for future MoS<sub>2</sub> nanopore studies.

## Materials and methods

### Supporting substrate fabrication

Substrates consisting of stacked layers of Al<sub>2</sub>O<sub>3</sub> and SiN<sub>x</sub> are fabricated on  $300 \pm 2$   $\mu\text{m}$  thick double-side polished (100) silicon wafers purchased from Silicon Quest International. Wafers are piranha cleaned (2:1 H<sub>2</sub>SO<sub>4</sub>/H<sub>2</sub>O<sub>2</sub>) for 20 min before deposition of SiN<sub>x</sub>. 300 nm of low-stress SiN<sub>x</sub> is deposited (STS Mesc PECVD system) using a mixed-frequency recipe (high frequency, 6 s at 13.56 MHz, platen power of 20 W; low frequency, 2 s at 380 kHz, platen power of 60 W) with precursors SiH<sub>4</sub> and NH<sub>3</sub> at flow rates of 40 and 55 sccm, respectively, at a platen temperature of 300 °C. Subsequently, 20 nm of Al<sub>2</sub>O<sub>3</sub> was deposited *via* ALD (Cambridge Nanotech) at a platen temperature of 250 °C using tetramethyl-aluminum (TMA) and water vapor precursors. Optical lithography is used to define square windows of 80  $\mu\text{m}$  on the back side of the wafer with the aid of plasma resistant Megaposit SPR-220 photoresist and an ABM Flood Exposure (model 60) tool. Then the wafer is placed inside an STS Pegasus ICP (inductively coupled plasma) DRIE and 80  $\mu\text{m}$  square membranes are suspended using a Bosch etching process; 500 to 600 nm holes are then drilled in these membranes using a focused ion beam (FIB) (FEI DB235) operated at a beam current of 30 pA.

### Chemical vapor deposition of molybdenum disulfide

The detailed processes of growing and characterizing the MoS<sub>2</sub> film using Chemical Vapor Deposition on SiO<sub>2</sub> and Sapphire substrates are described in previous studies.<sup>50,51</sup>

### Nanopore fabrication, chemicals, and materials

Single nanopores of various diameters were drilled in the free standing MoS<sub>2</sub> membrane on the supporting substrate





- 10 A. P. Feinberg, C. W. Gehrke, K. C. Kuo and M. Ehrlich, Reduced genomic 5-methylcytosine content in human colonic neoplasia, *Cancer Res.*, 1988, **48**(5), 1159–1161.
- 11 A. Murrell, V. K. Rakyan and S. Beck, From genome to epigenome, *Hum. Mol. Genet.*, 2005, **14**(suppl. 1), R3–R10.
- 12 A. Murrell, V. K. Rakyan and S. Beck, From genome to epigenome, *Hum. Mol. Genet.*, 2005, **14**(Spec. No. 1), R3–R10.
- 13 C. Grunau, E. Renault, A. Rosenthal and G. Roizes, MethDB—a public database for DNA methylation data, *Nucleic Acids Res.*, 2001, **29**(1), 270–274.
- 14 J. B. Kisiel, T. C. Yab, W. R. Taylor, S. T. Chari, G. M. Petersen, D. W. Mahoney and D. A. Ahlquist, Stool DNA testing for the detection of pancreatic cancer Assessment of Methylation Marker Candidates, *Cancer*, 2012, **118**(10), 2623–2631.
- 15 R. Kandimalla, A. A. van Tilborg and E. C. Zwarthoff, DNA methylation-based biomarkers in bladder cancer, *Nat. Rev. Urol.*, 2013, **10**(6), 327–335.
- 16 J. Shim, G. I. Humphreys, B. M. Venkatesan, J. M. Munz, X. Zou, C. Sathe, K. Schulten, F. Kosari, A. M. Nardulli, G. Vasmatzis and R. Bashir, Detection and Quantification of Methylation in DNA using Solid-State Nanopores, *Sci. Rep.*, 2013, **3**, 1389.
- 17 J. Shim, Y. Kim, G. I. Humphreys, A. M. Nardulli, F. Kosari, G. Vasmatzis, W. R. Taylor, D. A. Ahlquist, S. Myong and R. Bashir, Nanopore-Based Assay for Detection of Methylation in Double-Stranded DNA Fragments, *ACS Nano*, 2015, **9**(1), 290–300.
- 18 T. A. Desai, D. J. Hansford, L. Kulinsky, A. H. Nashat, G. Rasi, J. Tu, Y. Wang, M. Zhang and M. Ferrari, Nanopore Technology for Biomedical Applications, *Biomed. Microdevices*, 1999, **2**(1), 11–40.
- 19 V. Kurz, E. M. Nelson, J. Shim and G. Timp, Direct visualization of single-molecule translocations through synthetic nanopores comparable in size to a molecule, *ACS Nano*, 2013, **7**(5), 4057–4069.
- 20 E. M. Nelson, V. Kurz, J. Shim, W. Timp and G. Timp, Using a nanopore for single molecule detection and single cell transfection, *Analyst*, 2012, **137**(13), 3020–3027.
- 21 G. V. Soni, A. Singer, Z. Yu, Y. Sun, B. McNally and A. Meller, Synchronous optical and electrical detection of biomolecules traversing through solid-state nanopores, *Rev. Sci. Instrum.*, 2010, **81**(1), 014301.
- 22 J. Feng, K. Liu, R. D. Bulushev, S. Khlybov, D. Dumcenco, A. Kis and A. Radenovic, Identification of single nucleotides in MoS<sub>2</sub> nanopores, *Nat. Nanotechnol.*, 2015, **10**(12), 1070–1076.
- 23 S. Banerjee, J. Shim, J. Rivera, X. Jin, D. Estrada, V. Solovyeva, X. You, J. Pak, E. Pop, N. Aluru and R. Bashir, Electrochemistry at the edge of a single graphene layer in a nanopore, *ACS Nano*, 2013, **7**(1), 834–843.
- 24 K. Liu, J. Feng, A. Kis and A. Radenovic, Atomically Thin Molybdenum Disulfide Nanopores with High Sensitivity for DNA Translocation, *ACS Nano*, 2014, **8**(3), 2504–2511.
- 25 C. A. Merchant, K. Healy, M. Wanunu, V. Ray, N. Peterman, J. Bartel, M. D. Fischbein, K. Venta, Z. Luo, A. T. C. Johnson and M. Drndić, DNA Translocation through Graphene Nanopores, *Nano Lett.*, 2010, **10**(8), 2915–2921.
- 26 M. Fyta, Threading DNA through nanopores for biosensing applications, *J. Phys.: Condens. Matter*, 2015, **27**(27), 273101.
- 27 H. Bayley, Nanopore Sequencing: From Imagination to Reality, *Clin. Chem.*, 2014, **61**(1), 25.
- 28 K. Venta, G. Shemer, M. Puster, J. A. Rodriguez-Manzo, A. Balan, J. K. Rosenstein, K. Shepard and M. Drndic, Differentiation of short, single-stranded DNA homopolymers in solid-state nanopores, *ACS Nano*, 2013, **7**(5), 4629–4636.
- 29 J. Li, D. Yu and Q. Zhao, Solid-state nanopore-based DNA single molecule detection and sequencing, *Microchim. Acta*, 2016, **183**(3), 941–953.
- 30 H. W. C. Postma, Rapid Sequencing of Individual DNA Molecules in Graphene Nanogaps, *Nano Lett.*, 2010, **10**(2), 420–425.
- 31 S. Garaj, S. Liu, J. A. Golovchenko and D. Branton, Molecule-hugging graphene nanopores, *Proc. Natl. Acad. Sci. U. S. A.*, 2013, **110**(30), 12192–12196.
- 32 C. Sathe, X. Zou, J.-P. Leburton and K. Schulten, Computational Investigation of DNA Detection Using Graphene Nanopores, *ACS Nano*, 2011, **5**(11), 8842–8851.
- 33 A. B. Farimani, K. Min and N. R. Aluru, DNA Base Detection Using a Single-Layer MoS<sub>2</sub>, *ACS Nano*, 2014, **8**(8), 7914–7922.
- 34 G. F. Schneider, S. W. Kowalczyk, V. E. Calado, G. Pandraud, H. W. Zandbergen, L. M. K. Vandersypen and C. Dekker, DNA Translocation through Graphene Nanopores, *Nano Lett.*, 2010, **10**(8), 3163–3167.
- 35 A. P. S. Gaur, S. Sahoo, M. Ahmadi, S. P. Dash, M. J. F. Guinel and R. S. Katiyar, Surface Energy Engineering for Tunable Wettability through Controlled Synthesis of MoS<sub>2</sub>, *Nano Lett.*, 2014, **14**(8), 4314–4321.
- 36 S. Banerjee, J. Wilson, J. Shim, M. Shankla, E. A. Corbin, A. Aksimentiev and R. Bashir, Slowing DNA Transport Using Graphene-DNA Interactions, *Adv. Funct. Mater.*, 2015, **25**(6), 936–946.
- 37 J. Shim, J. A. Rivera and R. Bashir, Electron beam induced local crystallization of HfO<sub>2</sub> nanopores for biosensing applications, *Nanoscale*, 2013, **5**(22), 10887–10893.
- 38 J. Feng, K. Liu, M. Graf, M. Lihter, R. D. Bulushev, D. Dumcenco, D. T. Alexander, D. Krasnozhan, T. Vuletich, A. Kis and A. Radenovic, Electrochemical Reaction in Single Layer MoS<sub>2</sub>: Nanopores Opened Atom by Atom, *Nano Lett.*, 2015, **15**(5), 3431–3438.
- 39 P. M. Das and R. Singal, DNA methylation and cancer, *J. Clin. Oncol.*, 2004, **22**(22), 4632–4642.
- 40 G. Strathdee and R. Brown, Aberrant DNA methylation in cancer: potential clinical interventions, *Expert Rev. Mol. Med.*, 2002, **4**(4), 1–17.
- 41 D. K. Vanaja, M. Ehrlich, D. Van den Boom, J. C. Cheville, R. J. Karnes, D. J. Tindall, C. R. Cantor and C. Y. Young, Hypermethylation of genes for diagnosis and risk stratification of prostate cancer, *Cancer Invest.*, 2009, **27**(5), 549–560.

- 42 D. P. Hoogerheide, S. Garaj and J. A. Golovchenko, Probing surface charge fluctuations with solid-state nanopores, *Phys. Rev. Lett.*, 2009, **102**(25), 256804.
- 43 H. F. Jorgensen, K. Adie, P. Chaubert and A. P. Bird, Engineering a high-affinity methyl-CpG-binding protein, *Nucleic Acids Res.*, 2006, **34**(13), e96.
- 44 M. Ehrlich, DNA hypomethylation in cancer cells, *Epigenomics*, 2009, **1**(2), 239–259.
- 45 C. Krausz, J. Sandoval, S. Sayols, C. Chianese, C. Giachini, H. Heyn and M. Esteller, Novel insights into DNA methylation features in spermatozoa: stability and peculiarities, *PLoS One*, 2012, **7**(10), e44479.
- 46 M. Wanunu, W. Morrison, Y. Rabin, A. Y. Grosberg and A. Meller, Electrostatic focusing of unlabelled DNA into nanoscale pores using a salt gradient, *Nat. Nanotechnol.*, 2010, **5**(2), 160–165.
- 47 M. Waugh, A. Carlsen, D. Sean, G. W. Slater, K. Briggs, H. Kwok and V. Tabard-Cossa, Interfacing solid-state nanopores with gel media to slow DNA translocations, *Electrophoresis*, 2015, **36**(15), 1759–1767.
- 48 B. Kyle, C. Martin, K. Harold, L. Timothea, C. Sanmeet, B. José, W. Matthew and T.-C. Vincent, Kinetics of nanopore fabrication during controlled breakdown of dielectric membranes in solution, *Nanotechnology*, 2015, **26**(8), 084004.
- 49 L. Franceschini, T. Brouns, K. Willems, E. Carlon and G. Maglia, DNA Translocation through Nanopores at Physiological Ionic Strengths Requires Precise Nanoscale Engineering, *ACS Nano*, 2016, **10**(9), 8394–8402.
- 50 D. Dumcenco, D. Ovchinnikov, K. Marinov, P. Lazic, M. Gibertini, N. Marzari, O. Lopez Sanchez, Y. C. Kung, D. Krasnozhan, M. W. Chen, S. Bertolazzi, P. Gillet, A. Fontcuberta i Morral, A. Radenovic and A. Kis, Large-Area Epitaxial Monolayer MoS<sub>2</sub>, *ACS Nano*, 2015, **9**(4), 4611–4620.
- 51 K. K. H. Smithe, C. D. English, S. V. Suryavanshi and E. Pop, Intrinsic electrical transport and performance projections of synthetic monolayer MoS<sub>2</sub> devices, *2D Mater.*, 2017, **4**(1), 011009.
- 52 X. J. Lu and W. K. Olson, 3DNA: a software package for the analysis, rebuilding and visualization of three-dimensional nucleic acid structures, *Nucleic Acids Res.*, 2003, **31**(17), 5108–5121.
- 53 I. Ohki, N. Shimotake, N. Fujita, J.-G. Jee, T. Ikegami, M. Nakao and M. Shirakawa, Solution Structure of the Methyl-CpG Binding Domain of Human MBD1 in Complex with Methylated DNA, *Cell*, 2001, **105**(4), 487–497.
- 54 L. Kale, R. Skeel, M. Bhandarkar, R. Brunner, A. Gursoy, N. Krawetz, J. Phillips, A. Shinozaki, K. Varadarajan and K. Schulten, NAMD2: Greater scalability for parallel molecular dynamics, *J. Comput. Phys.*, 1999, **151**(1), 283–312.
- 55 A. D. MacKerell, D. Bashford, M. Bellott, R. L. Dunbrack, J. D. Evanseck, M. J. Field, S. Fischer, J. Gao, H. Guo, S. Ha, D. Joseph-McCarthy, L. Kuchnir, K. Kuczera, F. T. K. Lau, C. Mattos, S. Michnick, T. Ngo, D. T. Nguyen, B. Prodhom, W. E. Reiher, B. Roux, M. Schlenkrich, J. C. Smith, R. Stote, J. Straub, M. Watanabe, J. Wiorcikiewicz-Kuczera, D. Yin and M. Karplus, All-atom empirical potential for molecular modeling and dynamics studies of proteins, *J. Phys. Chem. B*, 1998, **102**(18), 3586–3616.
- 56 W. L. Jorgensen, J. Chandrasekhar, J. D. Madura, R. W. Impey and M. L. Klein, Comparison of simple potential functions for simulating liquid water, *J. Chem. Phys.*, 1983, **79**(2), 926–935.
- 57 U. Essmann, L. Perera, M. L. Berkowitz, T. Darden, H. Lee and L. G. Pedersen, A smooth particle mesh Ewald method, *J. Chem. Phys.*, 1995, **103**(19), 8577–8593.
- 58 S. E. Feller, Y. Zhang, R. W. Pastor and B. R. Brooks, Constant pressure molecular dynamics simulation: The Langevin piston method, *J. Chem. Phys.*, 1995, **103**(11), 4613–4621.
- 59 H. Qiu, A. Sarathy, K. Schulten and J.-P. Leburton, Detection and mapping of DNA methylation with 2D material nanopores, *njp 2D Mater. Appl.*, 2017, **1**(1), 3.



# Detection of Methylation on dsDNA using Nanopores in MoS<sub>2</sub> Membrane

## Supporting Information

Jiwook Shim<sup>1, #, \*</sup>, Shouvik Banerjee<sup>2, #</sup>, Hu Qiu<sup>3</sup>, Kirby K. H. Smithe<sup>4</sup>, David Estrada<sup>5</sup>, Julian Bello<sup>1</sup>, Eric Pop<sup>4</sup>, Klaus Schulten<sup>6</sup>, and Rashid Bashir<sup>7, 8, 9, \*</sup>

<sup>1</sup>Department of Biomedical Engineering, Rowan University, Glassboro, NJ 08028

<sup>2</sup>Department of Material Science and Engineering, University of Illinois at Urbana – Champaign, Urbana, IL 61801

<sup>3</sup>State Key Laboratory of Mechanics and Control of Mechanical Structures, Nanjing University of Aeronautics and Astronautics, Nanjing, 210016, China

<sup>4</sup>Department of Electrical Engineering, Stanford University, Stanford, CA 94305

<sup>5</sup>Department of Material Science and Engineering, Boise State University, Boise, ID 83725

<sup>6</sup>Department of Physics and Beckman Institute, University of Illinois at Urbana – Champaign, Urbana, IL 61801

<sup>7</sup>Department of Bioengineering, University of Illinois at Urbana – Champaign, Urbana, IL 61801

<sup>8</sup>Micro and Nanotechnology Laboratory, University of Illinois at Urbana – Champaign, Urbana, IL 61801

<sup>9</sup>Carle Illinois College of Medicine, University of Illinois at Urbana – Champaign, Urbana, IL 61801

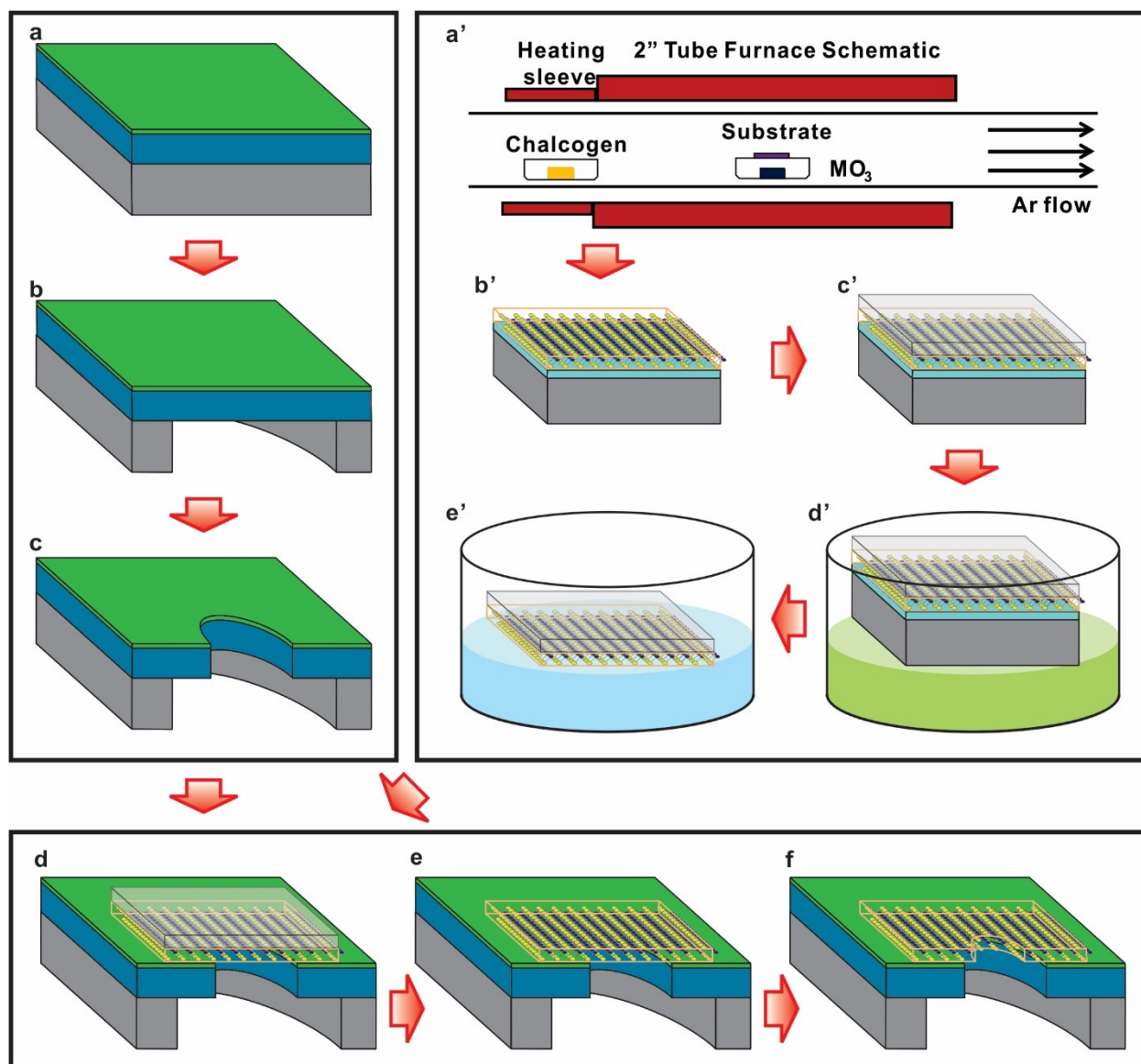


Figure S1. Detailed process of fabricating free-standing  $\text{MoS}_2$  membrane nanopore on the supporting substrate. a. Membranes consisting of stacked layers of  $\text{SiN}_x$  and  $\text{Al}_2\text{O}_3$  are fabricated on  $300 \pm 2 \mu\text{m}$  thick double-side polished  $\langle 100 \rangle$  silicon wafers purchased from Silicon Quest international. Before deposition of stacked layers, wafers are piranha cleaned (2:1  $\text{H}_2\text{SO}_4/\text{H}_2\text{O}_2$ ) for 20 min on a  $120^\circ\text{C}$  hotplate. 300 nm of low-stress  $\text{SiN}_x$  is deposited using STS Mesc PECVD system on the silicon substrate at a mixed-frequency recipe (high frequency, 6 s at 13.56 Mhz, platen power of 20 W; and low frequency, 2 s at 380 kHz, platen power of 60W) with precursors  $\text{SiH}_4$  and  $\text{NH}_3$  at flow rates of 40 and 55 sccm, respectively, at a platen temperature of  $300^\circ\text{C}$ . Subsequently 20 nm-thick  $\text{Al}_2\text{O}_3$  was deposited at a platen temperature of  $250^\circ\text{C}$  via ALD (Cambridge Nanotech) using tetramethyl-aluminum (TMA) and water vapor precursors. b. Optical lithography is used to define  $80 \mu\text{m}$  square windows on the back side of the wafer with the aid of plasma resistant megaposit SPR-220 photoresist and an ABM Flood Exposure (Model 60) tool. The wafer is then placed inside an STS Pegasus ICP DRIC and  $80 \mu\text{m}$  square membranes are suspended using a Bosch etching process. c. 500 to 600 nm holes are sculpted in these membranes using a focused ion beam (FIB, FEI DB235) operated at a beam current of 30 pA. a'. For  $\text{MoS}_2$  growth, the substrate is placed face-down over a crucible

containing ~1 mg of MoO<sub>3</sub> powder, and solid sulfur pieces are placed ~26 cm upstream. After evacuating the tube to <1 Torr, the tube is filled to 760 Torr with Ar. The Ar flow is then reduced to 30 sccm for the growth. Synthesis on SiO<sub>2</sub> is done as in Ref. S1, whereas synthesis on sapphire was done in a similar manner as Ref. S2. b'. The MoS<sub>2</sub> film is then removed from the furnace. c'. PMMA (A4 950K) is coated on the MoS<sub>2</sub> film by using spin coater at 3000 rpm followed by baking at 200 °C for 10 min. After 15 min cooling down, second PMMA layer was coated using the same parameters. d'. PMMA coated MoS<sub>2</sub> film on SiO<sub>2</sub> or Sapphire substrate was then floated on the 1M KOH at 80 °C for 1 hour till MoS<sub>2</sub>/PMMA stack delaminates. e' PMMA coated MoS<sub>2</sub> film is detached from the substrate. d. The detached PMMA/ MoS<sub>2</sub> layers are transferred to supporting substrate after rinsing with DIH<sub>2</sub>O, and dried at room temperature for 2 hours. Subsequently, the substrate is placed on a hot plate at room temperature and ramp to 150 °C for 20 min. e. The PMMA layer was dissolved in acetone for 30 min, rinsed with IPA, washed with DIH<sub>2</sub>O. Then, the samples are heated in Ar/H<sub>2</sub> atmosphere for 1.5 hours at 400 °C. f. A nanopore was drilled on the MoS<sub>2</sub> membrane as dscribed in Methods.



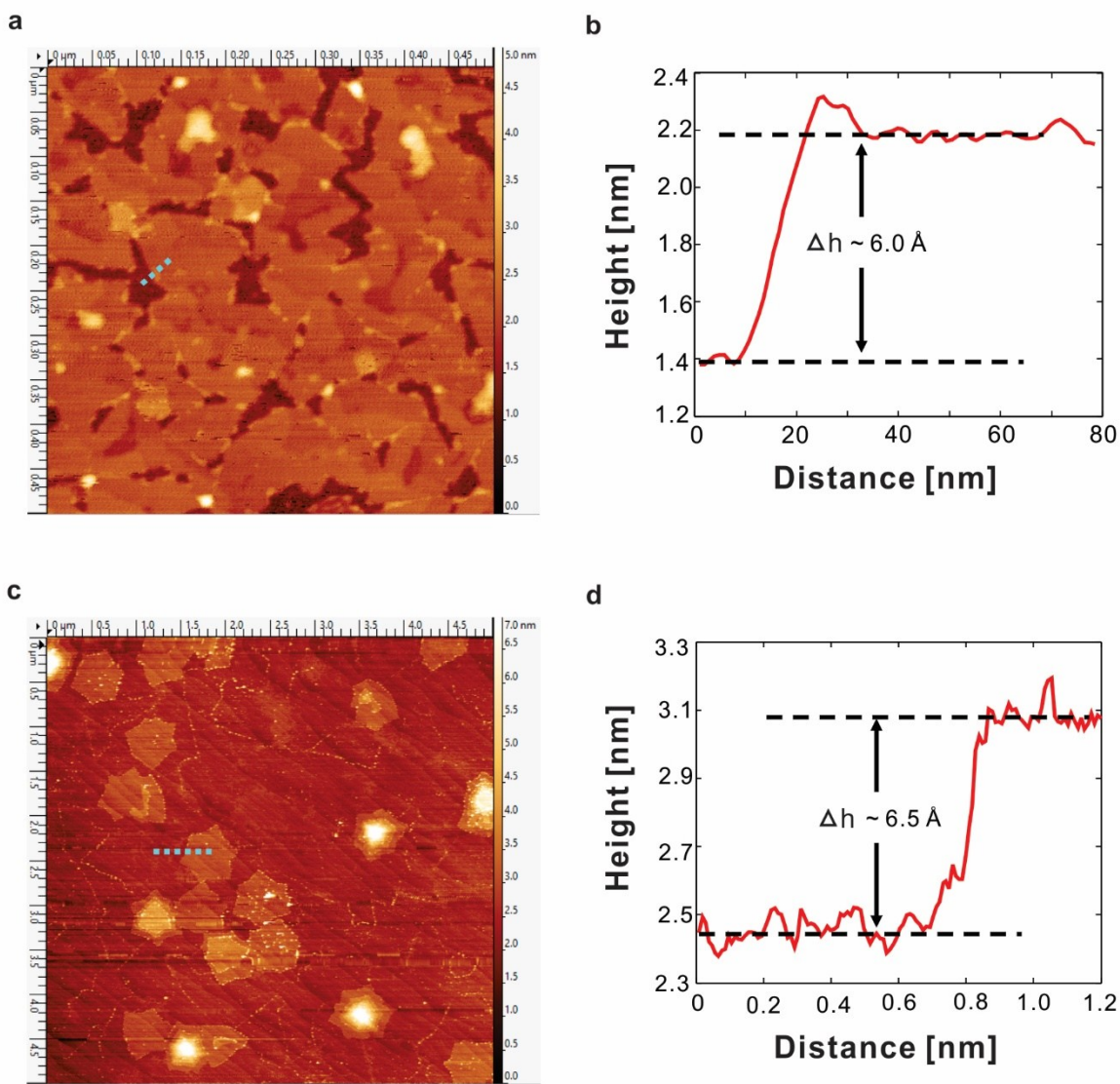


Figure S2. (a) and (b): AFM image and height profile of a subcontinuous MoS<sub>2</sub> growth on sapphire showing the monolayer height of  $\sim 6 \text{ \AA}$ . (c) and (d): AFM image and height profile of a continuous growth on sapphire, showing small overgrowth regions with a 1L-2L height of  $\sim 6.5 \text{ \AA}$ . Also note the ridges in Fig. S2c, which are the terraces of the reconstructed sapphire surface, as in Ref. S2.

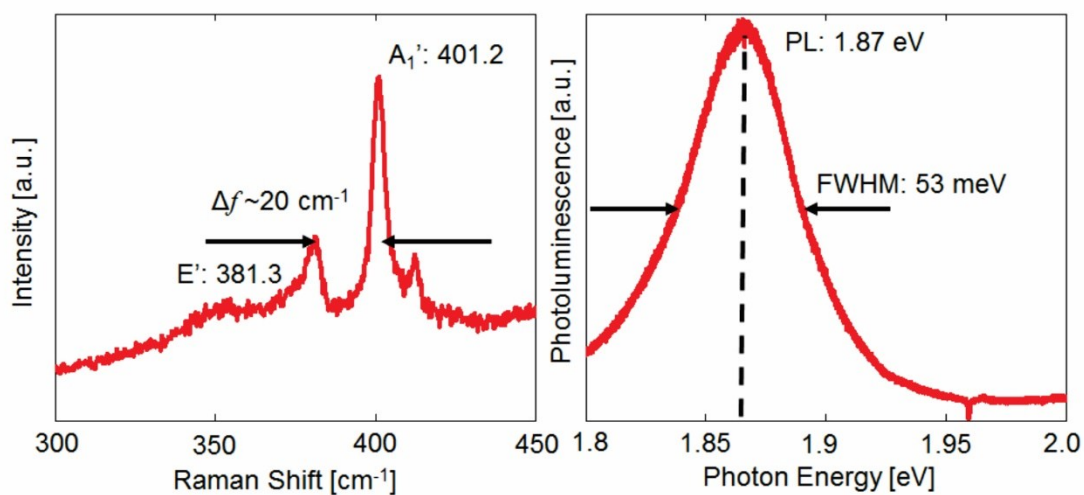


Figure S3. Raman (left) and photoluminescence (right) data for as-grown 1L MoS<sub>2</sub> on sapphire. In the Raman spectrum, the E' and A<sub>1</sub>' vibrational modes are near 381 and 401 cm<sup>-1</sup>, respectively. The PL spectrum has a peak near 1.87 eV and FWHM of 53 meV.

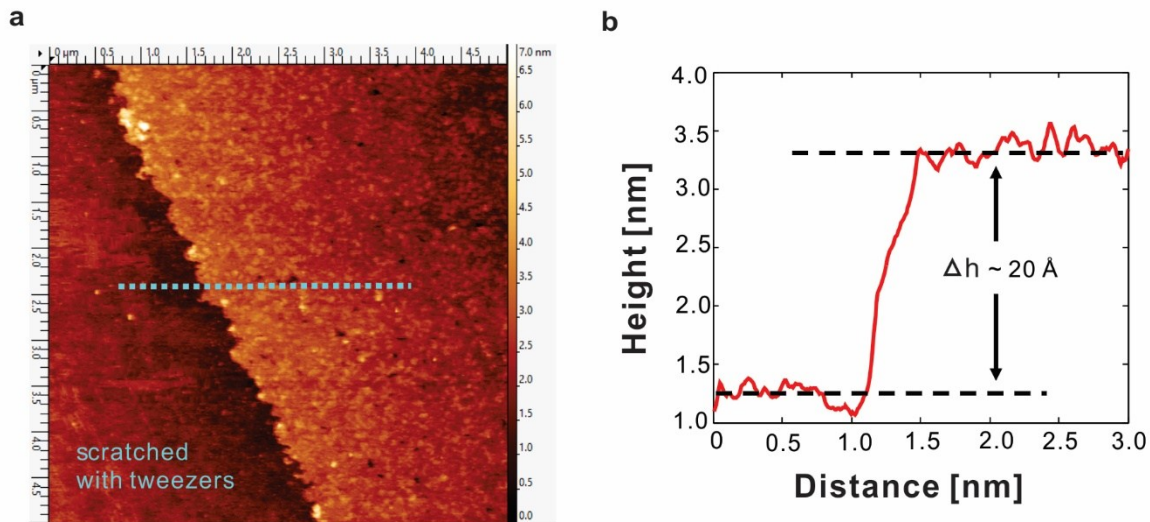


Figure S4. (a) and (b): AFM image and height profile of a continuous growth on  $\text{SiO}_2$ . The measured step height here is  $\sim 20 \text{ \AA}$  due to the bare surface being made by scratching the  $\text{MoS}_2$  away with tweezers.



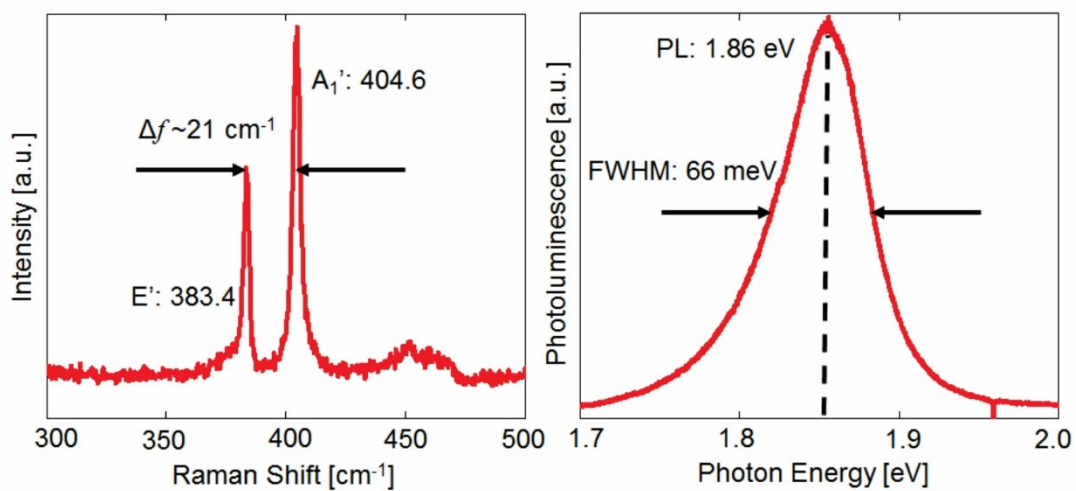


Figure S5. Raman (left) and photoluminescence (right) data for continuous MoS<sub>2</sub> grown on SiO<sub>2</sub>. In the Raman spectrum, the E' and A<sub>1</sub>' vibrational modes are near 383.5 and 404.5 cm<sup>-1</sup>, respectively. The PL spectrum has a peak near 1.86 eV and FWHM of 66 meV.

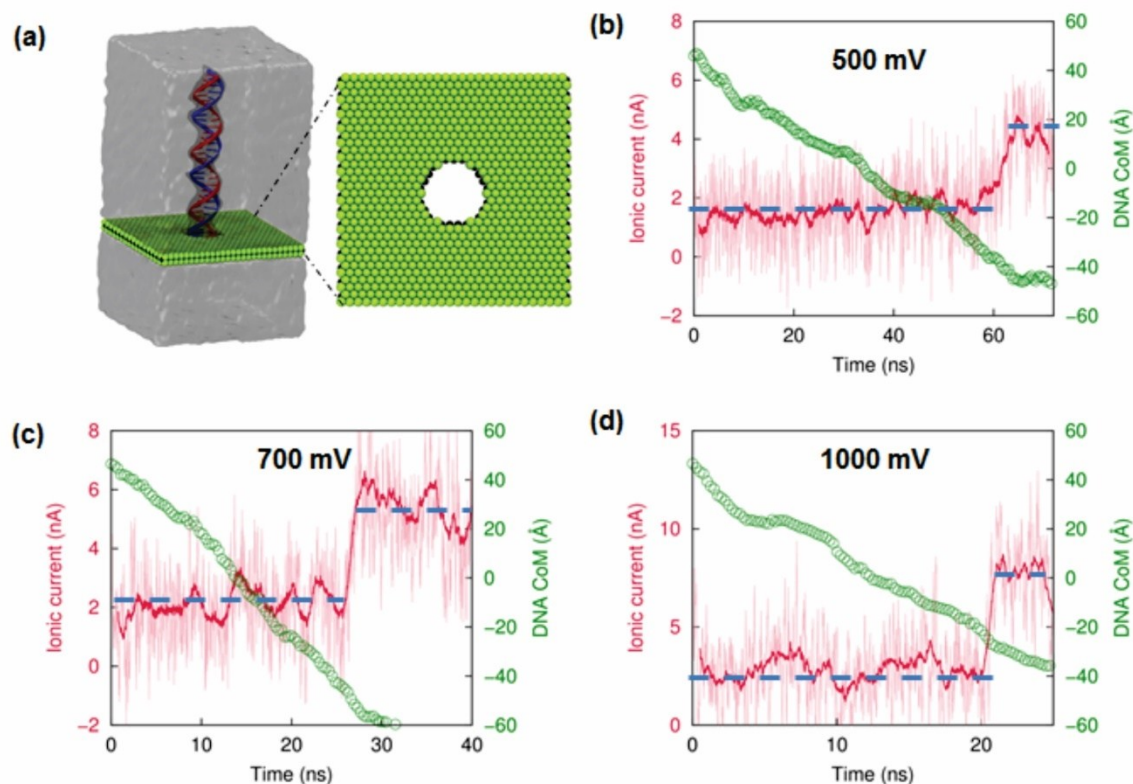


Figure S6. Molecular dynamics simulation of dsDNA translocation through a 2.4 nm diameter MoS<sub>2</sub> nanopore under different voltage biases. (a) Simulation system consisting of a monolayer MoS<sub>2</sub> and a 30 bp long dsDNA strand embedded in a 1 M NaCl solution. (b-c) Recorded ionic current (red) and the center of mass positions of the DNA molecule (green circles) in the direction perpendicular to the MoS<sub>2</sub> membrane when an transmembrane voltage 500 (b), 700 (c), 1000 (d) mV was applied to drive the dsDNA translocation through the pore.

To explore the atomic-scale translocation dynamics of a dsDNA through MoS<sub>2</sub> nanopore, we performed three independent molecular dynamics simulations on the system shown in Figure S6a under voltage biases of 500, 700, 1000 mV, respectively. It is found that the recorded ionic current when the pore is occupied by DNA is evidently lower than the open pore current in all the simulations, showing successful detection of DNA translocation (Figure S6c-d), in agreement with our experimental observation.

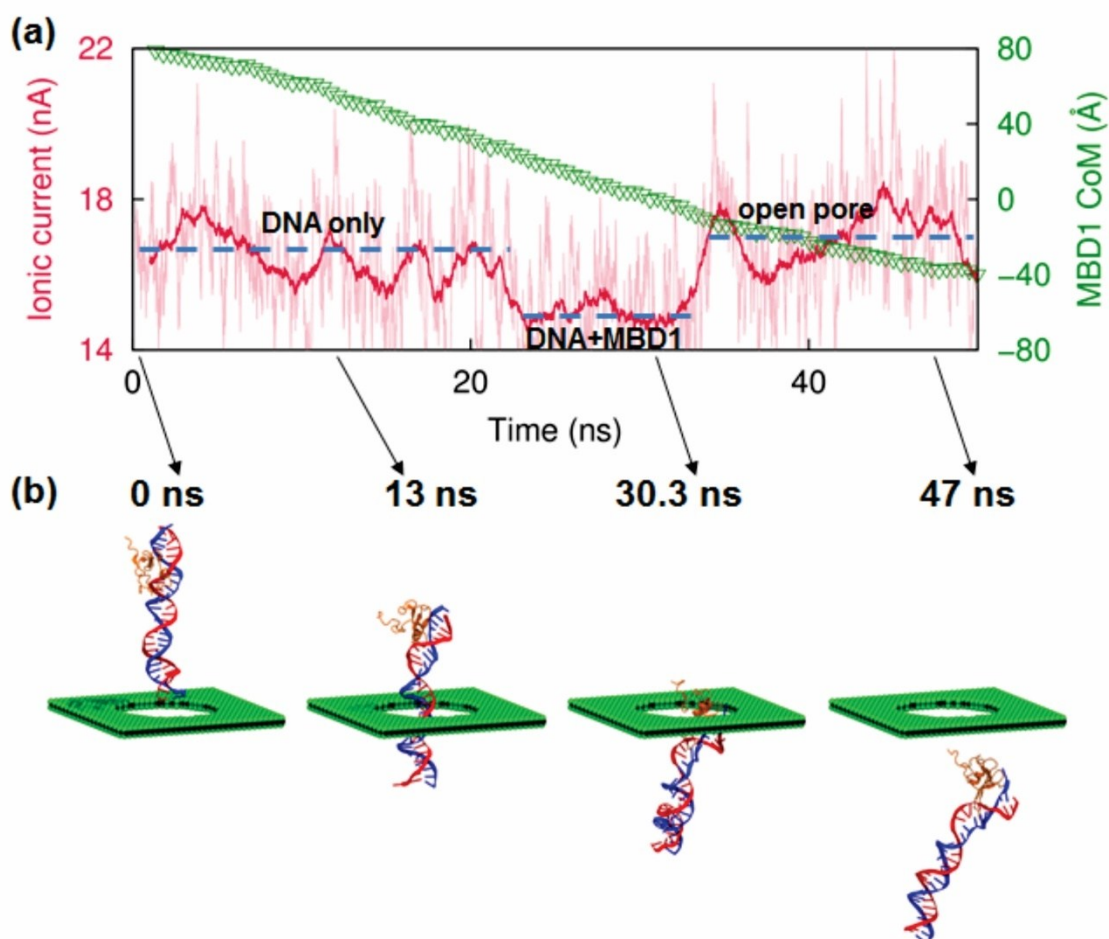


Figure S7. Molecular dynamics simulation of a DNA-MBD1 complex translocation through a 6 nm diameter MoS<sub>2</sub> nanopore under a 500 mV voltage bias. (a) Recorded ionic current (red) and the center of mass position of the MBD1 protein (green triangles) during the translocation of the complex. (b) Snapshots of the MD trajectory at different time instants

We also performed molecular dynamics simulations to study on the atomic-scale the translocation process of a terminal-methDNA/MBD1 complex through a MoS<sub>2</sub> nanopore, as shown in Figure S7. The recorded ionic current exhibits clearly three subsequent levels, ~16.7, ~15 and ~17 nA, induced by the occupation of the pore by DNA only, DNA plus MBD1 protein and nothing (i.e., open pore), respectively. This finding suggests detection of the MBD1 protein and the associated methylation sites.

Supplementary Information Figure S8

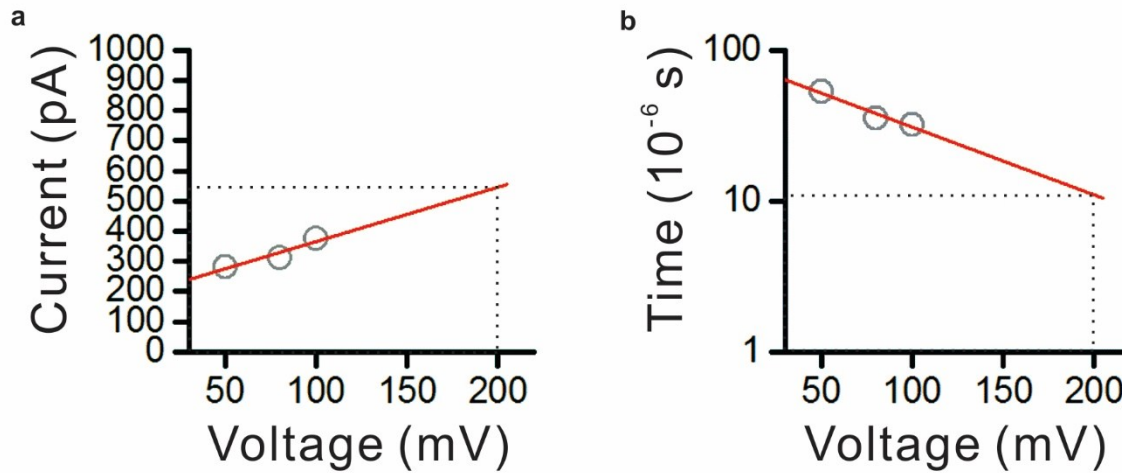


Figure S8. Expected blocked current level and current blockage duration for translocation of 90 bp double-stranded DNA through 7.2 nm MoS<sub>2</sub> nanopore at 200 mV. a. Blocked current at 200 mV was obtained by fitting first-order Polynomial to blocked current values at 50 mV, 80 mV, and 100 mV, and extended the fitting trend to 200 mV. b. Transport duration of 90 bp dsDNA at 200 mV was obtained by fitting Exponential decay function to transport duration value at 50 mV, 80 mV, and 100 mV, and extended the fitting trend to 200 mV.



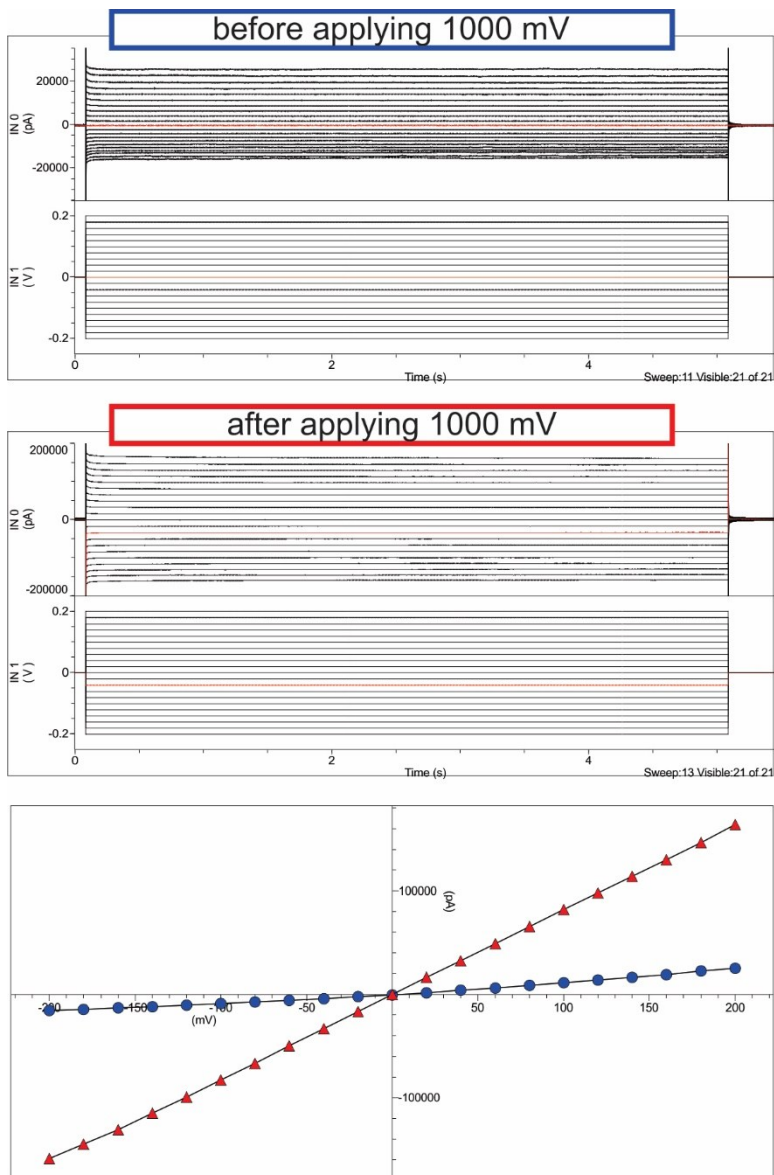


Figure S9. Enlargement of a MoS<sub>2</sub> nanopore. The top figure shows the initial IV curve characteristic of a MoS<sub>2</sub> nanopore before applying 1000 mV. The middle figure shows the IV curve characteristic of the MoS<sub>2</sub> nanopore after exposed at 1000 mV for multiple times. The bottom figure shows the difference of IV characteristic between before and after applying the biased voltage of 1000 mV.

[S1] K. K. H. Smithe, C. D. English, S. V Suryavanshi, and E. Pop, *2D Mater.* **4**, 1 (2017). DOI: 10.1088/2053-1583/4/1/011009.

[S2] D. Dumcenco, D. Ovchinnikov, K. Marinov, P. Lazić, M. Gibertini, N. Marzari, O. L. Sanchez, Y.-C. Kung, D. Krasnozhan, M.-W. Chen, S. Bertolazzi, P. Gillet, A. Fontcuberta i Morral, A. Radenovic, and A. Kis, *ACS Nano* **9**, 4611 (2015). DOI: 10.1021/acsnano.5b01281.